Hadronic Calorimetry and Jet/τ/E$_T^{miss}$ Performance Studies in ATLAS

B. Caron
on behalf of the ATLAS Collaboration

Centre for Subatomic Research
Department of Physics
University of Alberta
Edmonton, AB Canada T6G 2N5
e-mail: caron@phys.ualberta.ca

Abstract. Jets, τ jets, and missing transverse energy are important components of the physics expected at the LHC. The accurate measurement of the direction and energy of jets, along with missing energy, impose strong requirements upon the performance of the ATLAS detector system. These requirements and the ATLAS Hadronic Calorimetry system are reviewed. A brief discussion of the jet reconstruction algorithms, jet energy scale calibration, and forward jet tagging is also included. The methods and expected accuracy by which τ jets are reconstructed and identified is covered. The expected E_T^{miss} resolution and minimization of fake high E_T^{miss} tails is presented.

1 Introduction

The observation of jets, τ jets, and missing transverse energy (E_T^{miss}) play important roles in the physics to be observed at the LHC. These objects are additionally important since they are also signatures for new physics beyond the Standard Model, such as Supersymmetry and compositeness.

Jets are used in many fashions in the study of various physics channels. These include the reconstruction of resonances such as $W \to jj$, $Z \to b\bar{b}$ or $t \to bW$, the measurement of jet multiplicities, background rejection through jet vetoes in the central region, forward tagging of jets, and QCD studies.

Good measurement of E_T^{miss} is necessary at the LHC since it is an important signature for new physics , i.e. the production and decay of SUSY particles, as well as the production and decay of a Higgs boson. Therefore good calorimeter performance in terms of energy resolution, response linearity and hermeticity is needed to reconstruct narrow invariant mass distributions for new heavy particles involving neutrinos among their decay products, such as from $A \to \tau\tau$.

2 ATLAS Calorimetry

In order to achieve its ambitious physics goals, the ATLAS calorimetry [1, 2] was designed with the following performance requirements:

- Energy resolution $\frac{\sigma(E)}{E} = \frac{50\%}{\sqrt{E}} \oplus 3\%$ within the central rapidity region $|\eta| < 3$;

- Energy resolution $\frac{\sigma(E_T)}{E_T} < 10\%$ for $E_T > 100$ GeV clusters in the forward region $3 < |\eta| < 5$;

- 1% precision in the measurement of the absolute jet energy scale;

- jet tagging efficiency greater than 90%;

- granularity of $\delta\eta \times \delta\phi = 0.1 \times 0.1$ within the central region, $|\eta| < 3$, adapted to the lateral hadron shower size.

A 3-dimensional view of the calorimeter system is presented in Figure 1. Hadron calorimetry is present in the barrel (Hadronic Tile), end-cap (Hadronic Liquid Argon End-cap) and forward (Hadronic Liquid Argon Forward) regions of the detector.
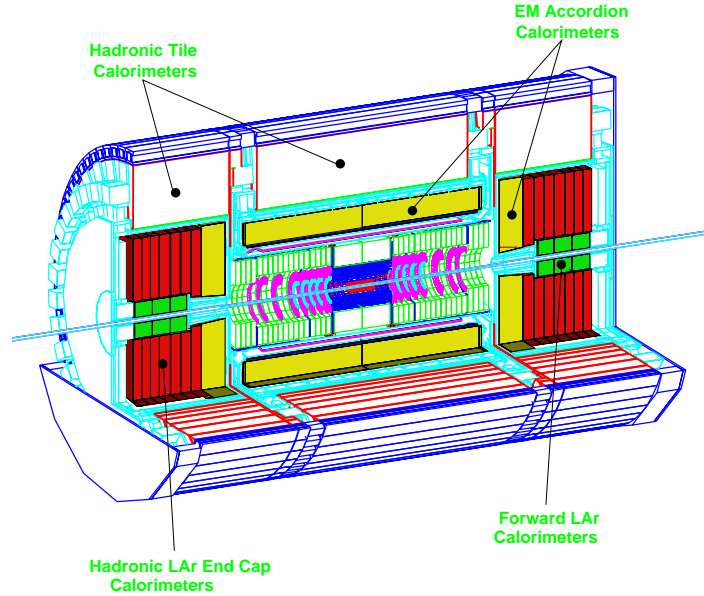

Fig. 1. 3-Dimensional cut-out view of the ATLAS Calorimeter system which is approximately 13.3 m in length and 8.5 m in height.

2.1 Hadronic Tile Calorimeter

The Hadronic Tile Calorimeter consists of modules of iron absorber and scintillator tile readout with a granularity of $\Delta\eta \times \Delta\phi = 0.1 \times 0.3$. There are three longitudinal samplings, providing coverage over the region of $|\eta| < 1.7$.

2.2 Hadronic Liquid Argon End-cap Calorimeter

The Hadron Liquid Argon (LAr) End-cap Calorimeter consists of copper absorbers arranged in a parallel plate geometry. A total of four longitudinal samplings provide coverage down to $|\eta| < 3.2$. The granularity of the samplings varies with the region of coverage, with $\Delta\eta \times \Delta\phi \approx 0.1 \times 0.1$ within $1.5 < |\eta| < 2.5$, and $\Delta\eta \times \Delta\phi \approx 0.2 \times 0.2$ within $2.5 < |\eta| < 3.2$.

2.3 Hadronic Liquid Argon Forward Calorimeter

The Hadronic LAr Forward Calorimeter consists of 3 modules. The electromagnetic module is closest to the interaction point and consists of copper absorber. The two remaining hadronic modules use tungsten as the absorber material. The modules are each 28, 91, and 89 radiation lengths in depth and provide nearly 2.7, 3.7, and 3.6 hadronic interaction lengths. The principal coverage provided by the Forward Calorimeter is between $3.1 < |\eta| < 4.9$ with non-projective readout cells covering an area of approximately $\Delta\eta \times \Delta\phi = 0.2 \times 0.2$. The Forward Calorimeter is fully integrated into the rest of the ATLAS calorimetry system, aiding to minimize any cracks in calorimeter coverage. This is a premium feature for physics measurements with the ATLAS Calorimetry.

3 Jet Reconstruction

Jet reconstruction is impacted by both physics effects, which are properties of each event, and detector features, which affect the detection details. Physics effects include fragmentation, initial and final state radiation, the underlying event, and minimum bias events. Detector features such as magnetic field, lateral shower size and calorimeter granularity, the presence of dead material and cracks between calorimeters, longitudinal shower leakage, and electronic noise influence the calorimeter performance.

3.1 Jet Algorithms

The two standard jet reconstruction algorithms used in ATLAS are the simple cone and K$_T$ clustering [4] algorithms. The cone algorithm utilizes the highest transverse energy (E$_T$) tower in the calorimeter for the jet seed and initial cone direction. The algorithm further iterates upon the cone direction and provides various methods to handle the overlapping, merging, and sharing of energy between jets. The K$_T$ cluster algorithm begins with the full set of final hadrons, approximated by towers in the calorimeter, and pairs them together progressively merging all towers into jets.

The influence of cone size on reconstructed jet energy and resolution is shown in Figure 2 [3]. The effects of pile-up and electronic noise are omitted from the plot. Out-of-cone loss due to fragmentation and magnetic field effects are evident for cone sizes of radius $\Delta R = 0.4$. Here the effect is purely statistical, and only increases the value of the sampling term. The high energy jets are only slightly affected since, due to the boost, the particles in the jet are more collimated and therefore better contained within the cone.
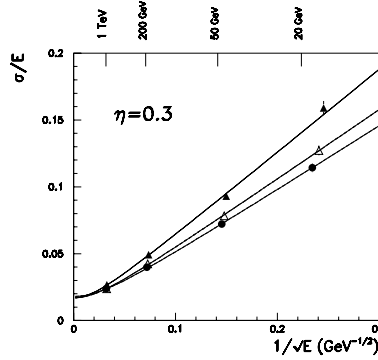

Fig. 2. Energy resolution for jet energies ranging from 20 GeV to 1 TeV at $|\eta| = 0.3$. Black circles, open triangles, and black triangles are obtained using energies summed in cone size of $\Delta R = 1.5$, 0.7, and 0.4, respectively.

3.2 Dead Material and Crack Regions

There are two main transition regions within the ATLAS Calorimetry. A transition between the barrel and end-cap hadronic calorimeters occurs within a vertical crack at $|\eta| \approx 1$ and at the end of the coil and corners of the cryostat walls at $|\eta| \approx 1.45$. A second transition region occurs at $|\eta| \approx 3.2$ between the hadronic end-cap and forward calorimeters. The transition regions are clearly visible in Figure 3 (left) [3] which shows the absorption length as a function of pseudorapidity.

In order to partially recover the energy loss, the crack region is instrumented with the Intermediate Tile Calorimeter (ITC) and additional scintillators. Calibration procedures also include weights for each calorimeter compartment with correction terms for the energy losses in the dead material, such as the cryostat. The energy loss as a function of pseudorapidity for a 200 GeV jet is shown in Figure 3 (right) [3].

3.3 Electronic Noise and Pile-up

The effect of electronic noise and pile-up on energy reconstruction has been studied for jets in the barrel region at $|\eta| = 0.3$. Figure 4 (left) [3] shows the fitted jet energy resolution for cone sizes of $\Delta R = 0.4, 0.7$ with and without
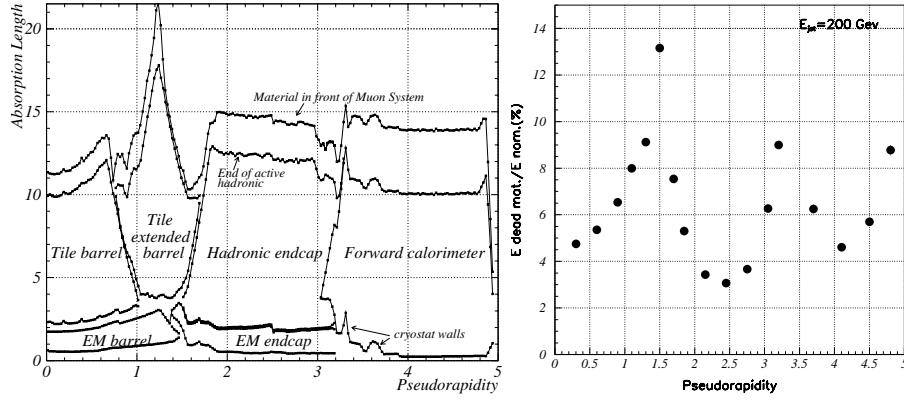
Fig. 3. Left Figure: Total thickness (in absorption lengths) of the ATLAS calorimetry as a function of pseudorapidity. Right Figure: Fractional energy loss of 200 GeV jets in dead material as a function of pseudorapidity.

the addition of electronic noise. Different cell energy cuts were used and the corresponding noise evaluated. The optimal cut value is dependent upon the jet energy as well as the cone size. The best overall performance was obtained for a 2.5σ cut.

Similarly the effect of pile-up from minimum bias events was studied. The jet energy resolutions obtained when accounting for pile-up is shown in Figure 4 (right) [3] for a cone size of $\Delta R = 0.4$. Once calibrated at the hadronic scale the equivalent noise term was found to be 4.7 GeV.
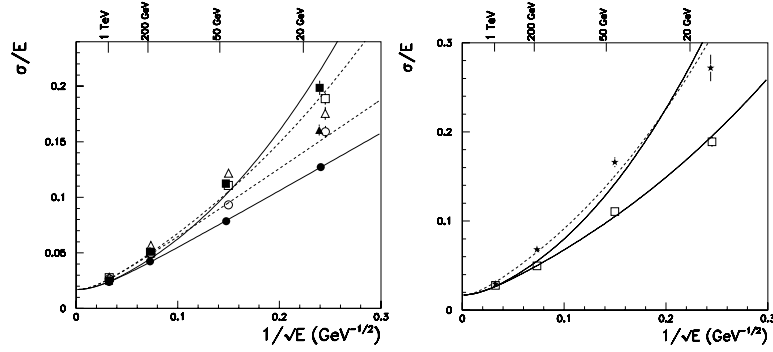

Fig. 4. Left Figure: Effect of the electronic noise on the jet energy resolution. Black dots (open dots) are for cone size $\Delta R = 0.7(0.4)$ and no electronic noise. Black squares (open squares) are for cone size $\Delta R = 0.7(0.4)$ with electronic noise. Black triangles (open triangles) are for cone size $\Delta R = 0.7(0.4)$ with 2.5σ cell energy cut. Right Figure: Jet energy resolution obtained with electronic noise and pile-up included for cone size $\Delta R = 0.4$.

3.4   Offline Jet Energy Calibration

The ATLAS calorimeters are not compensating and a calibration procedure has to be applied to determine the jet energy and improve the resolution. Several algorithms are available to calibrate the jet energies. The two main algorithms are the sampling-dependent weighting technique, with weights applied to the different calorimeter compartments, and the H1 based cell weighting approach, with weights applied directly to the calorimeter cell energies. In both cases corrections are made in order to take into account the energy loss which is deposited in the cryostat. With the cell weighting method the applied weights are parameterized functions which correct upwards the response of cells with small signal to make its response equal to that of cells with large, typically electromagnetic, deposited energy.

Figure 5 [3] shows the results obtained for the two calibration methods, with two different cone sizes, for back-to-back dijet events in the central barrel region ($|\eta| = 0.3$). In both cases the energy resolution improves only slightly with larger cone size due to the increased presence of electronic noise. In general, the cell weighting method provides a better energy resolution and smaller residual non-linearity ($\sim 2\%$) when compared to the sampling method ($\sim 3\%$).
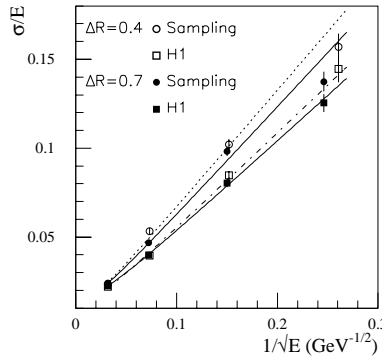

Fig. 5. Jet energy resolutions obtained with the sampling and cell weighting (H1 based) methods for two cone sizes.

3.5   ATLAS Test Beam Results

In addition to the use of detector simulation programs a great deal of effort has been made to study the response of both prototype and production calorimeter segments to single particles in test beam.

Combined tests of the electromagnetic LAr and hadronic Tile barrel calorimeter prototypes were performed in 1994 and 1996 [3]. Figure 6 (left) illustrates the obtained energy resolution for single pions of varying energy compared with the results from the G-$CALOR$ hadronic simulation package. The solid line depicts the energy dependence of the resolution parameterized using the equation

$$\frac{\sigma}{E} = \frac{a}{\sqrt{E}} \oplus b \oplus \frac{c}{E} \tag{1}$$

Here $a/\sqrt{E}$ is the sampling term, b is the constant term, and c/E is the noise term.

The energy dependence of the e/π ratio was also observed as part of the combined test beam. This energy dependence provides a measure of the degree of non-compensation of the calorimeter e/h which is the ratio of the calorimeter response to the electromagnetic and purely hadronic shower components. The relationship between e/h and e/π depends upon the electromagnetic fraction produced in the interaction:

$$\frac{e}{\pi} = \frac{e/h}{1 + (e/h - 1) \cdot f_\pi^0} \tag{2}$$

where f_π^0 is the mean fraction of initial π energy deposited via electromagnetic cascades and can be approximated as [5]

$$f_\pi^0 \approx 0.11 \cdot \ln E \tag{3}$$

where E is in GeV. Figure 6 (right) shows the fit results for both data and simulation. The G-CALOR simulation predicts a lower level of calorimeter non-compensation.
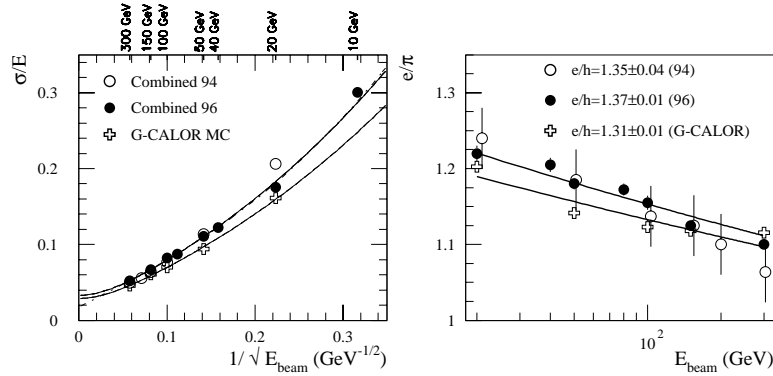

Fig. 6. Left Figure: Energy resolution for pions. Right Figure: Energy dependence of the e/π ratio.

To estimate the energy resolution for jets in the end-cap region modules of the ATLAS LAr Hadronic end-cap calorimeter (HEC) were exposed to beams of electrons, muons and pions in 2000 [6].

The energy dependence of the energy resolution for pions at one impact point on the HEC module can be found in Figure 7. Included in the figure is the prediction from G-CALOR. G-CALOR is slightly optimistic in its description of the energy resolution, as can be seen from the smaller value of the constant term.
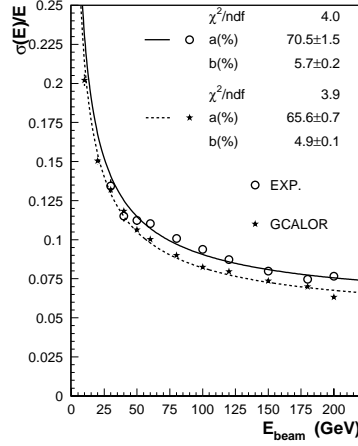
Fig. 7. Comparison of the energy dependence of the pion energy resolution with the prediction from simulation. Shown are the data (full dots) and G-CALOR hadronic shower simulation code prediction (stars).

For the analysis of the HEC test beam data the function f_π^0 was parameterized as [7]

$$f_\pi^0 = 1 - (\frac{E}{E_0'})^{m-1} \tag{4}$$

In the case of pions the values are typically $E_0' \approx 1$ GeV and $m \approx 0.85$. Figure 8 (a) demonstrates the measured e/π ratio for uncorrected data. The resulting e/π ratio after correcting for energy leakage is shown in Figure 8 (b). After fitting the data with Eqs. 2 and 4 the e/h ratio was found to be $e/h = 1.49 \pm 0.01$. When using the approximation given in Eq. 3 the quality of fit was degraded but still resulted in similar values of e/h.

The response of the Tile hadron calorimeter to muons was also extensively studied [3]. The ability to measure a clean muon signal above noise, particularly in the outermost compartment, is a valuable asset. In a high luminosity environment such as at the LHC, physics muons may overlap other particles and minimum bias events will deposit non-negligible amounts of energy in the inner-most calorimeter layers. Figure 9 shows the signal deposited by muons in all compartments (left) and in the outermost compartment (right) of the Tile Calorimeter module 0 by 100 GeV muons. The signal is well separated from the electronic noise which is depicted by the dashed lines. The electronic noise is at the level of ~ 40 MeV.
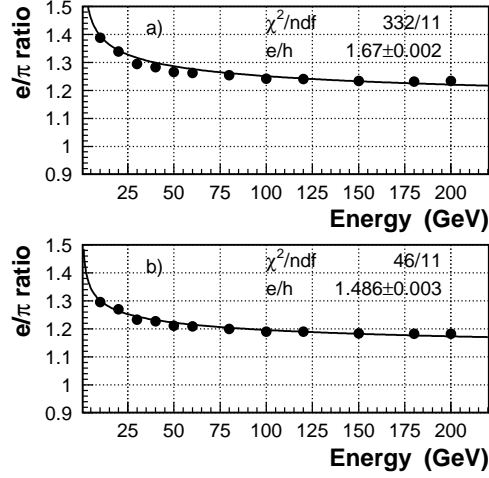
Fig. 8. The energy dependence of the e/π ratio for uncorrected data (a) and after correcting for energy leakage (b).
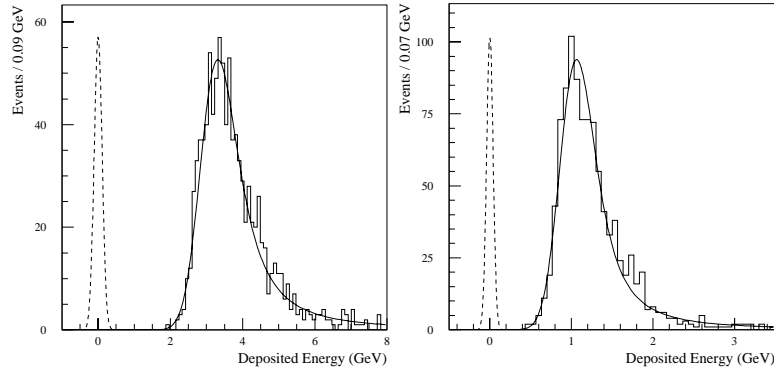

Fig. 9. Total deposited energy (left) and energy deposited in the third compartment (right) by 100 GeV muons in the Tile Calorimeter extended barrel module zero at $\eta = 1.3$. Dashed lines represent the electronic noise distributions.

3.6 Jet Energy Scale and Calibration

The aim of the ATLAS detector is to measure the absolute jet energy scale to the $\approx 1\%$ level.

An initial relative energy scale measurement will be possible through the measurement of E/p for isolated high p_T charged hadrons from τ decays [3]. In this measurement the energy scale calibration is transferred from test beam and

used to inter-calibrate the various calorimeters. Using this method it is possible to constrain the absolute energy measurement scale for isolated charged π's. However, from simulation it has been found that the track momentum measurement in the Inner Detector is not obviously matched to the calorimeter energy since it is not possible to completely reject $\pi^{\pm}$ which overlap with π^0. Using the fine granularity of the electromagnetic calorimeter the background of overlapping π^0 can be reduced. By rejecting events where energy is observed outside a cone size of $\Delta R = 0.025$, which is the size of a cell in the EM calorimeter, centered on the matching track, it is possible to reduce the bias imparted to the E/p distribution [3].

3.6.1   In Situ Jet Energy Calibration In situ jet energy calibration will be possible through the observation of $W \rightarrow j\,j$ decays from inclusive $t\bar{t}$ production [3]. Figure 10 (left) demonstrates the fraction of measured jet p_T carried by the parton as a function of the measured jet p_T before and after jet energy calibration is applied. For $p_T^{jet} > 70$ GeV a jet energy scale systematic uncertainty of $\pm 1\%$ is expected. Residual effects due to final state radiation arising from out-of-cone energy loss are at the level of 10% for jets with $p_T \approx 50$ GeV. For jets with $p_T > 200$ GeV the two jets are required to be separated by $\Delta R > 0.8$ to minimize jet overlap effects.

The $W \rightarrow j\,j$ sample can cleanly be separated from the large QCD (W+jet) and electroweak ($W\,W$) backgrounds by requiring the events contain an isolated lepton with $p_T > 20$ GeV and at least four jets with $p_T > 40$ GeV, and two of which are tagged as b-jets.

In situ jet energy calibration is also possible by observing the p_T balance between the highest p_T jet and leptonic Z decay from Z+jet events [3]. Figure 10 (right) shows the observed p_T balance. Through the application of a tight jet veto and requiring that the angle $\Delta\phi > 3.06$, it is possible to reach a $\pm 1\%$ sensitivity in the jet energy scale measurement.

3.7   Low p$_T$ Jet Reconstruction

The identification of low p_T jets can have a substantial impact upon the observed physics. It is important to be able to veto mult-jet final states where the jets are of low p_T. The presence of a low p_T jet veto is especially valuable when utilizing Z+jet(s) events for in situ calibration.

A central jet veto is particularly useful to reject $t\bar{t}$ backgrounds. Figure 11 [3] plots the jet veto efficiency as a function of the applied jet veto threshold for the simulation of a Heavy Higgs boson. Good efficiency and background rejection is expected for a 15 (25) GeV jet veto threshold when applied at low (high) luminosity. Further work is required to establish an experimental program to validate the physics model used in the simulation.

3.8   Forward Jet Tagging

The ability to perform forward jet tagging is important for the observation of Higgs boson production through Vector Boson Fusion [3]. Figure 12 illustrates
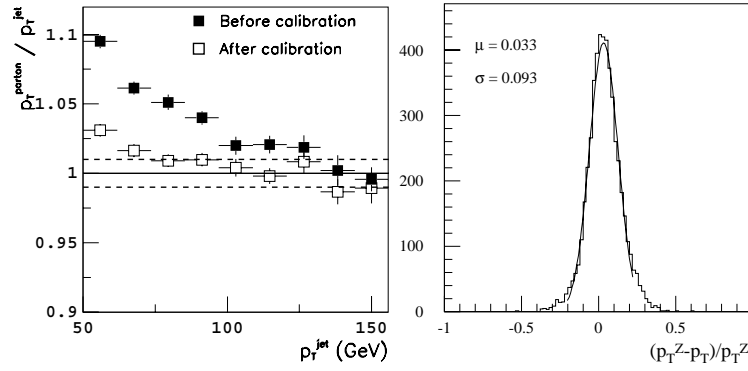
Fig. 10. Left Figure: Ratio of the original parton p_T, p_T^{parton}, to the p_T of the reconstructed jet, p_T^{jet}, as a function of p_T^{jet} for $W \to jj$ decays from inclusive $t\bar{t}$ events. Right Figure: Fractional imbalance between the p_T of the Z boson, p_T^Z, and the p_T of the leading jet for Z+jet events with a cone size of $\Delta R = 0.7$.
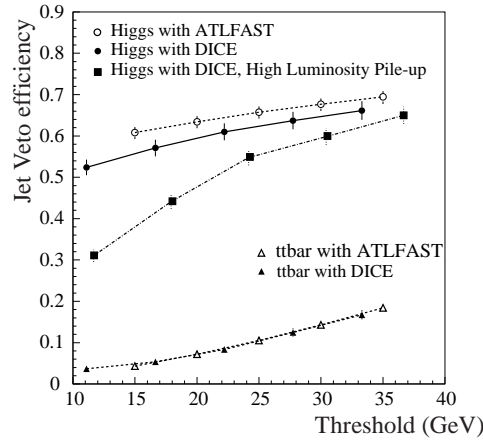

Fig. 11. Jet veto efficiency for the Higgs signal and the $t\bar{t}$ background obtained at particle level with parameterized fast simulation (ATLFAST) for low luminosity, and for low and high luminosity with full simulation (DICE).

the Feynman diagram for this process. In this process the two jets are observed within the region of $2 < |\eta| < 5$ covered by the end-cap and forward calorimeters. Figure 13 (top) shows the p_T distribution of the produced jets as a function of pseudorapidity for $M_H = 1000$ GeV.

A cut on the significance (ratio of the signal to the rms from noise) within a cone of size $\Delta R = 0.2$ around the seed cell yields an efficient discrimination between pile-up and signal jets in the Forward Calorimeter. Figure 13 (bottom)

demonstrates the expected tagging efficiency as a function of pseudorapidity. The tagging efficiency decreases by less than 10% when operating at high luminosity. A constant fake tag rate of $\approx 1(10)\%$ is achievable for double (single) jet tags within the $2 < |\eta| < 5$ coverage.
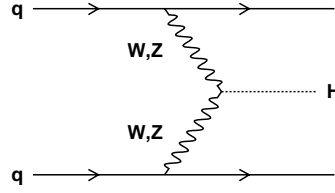

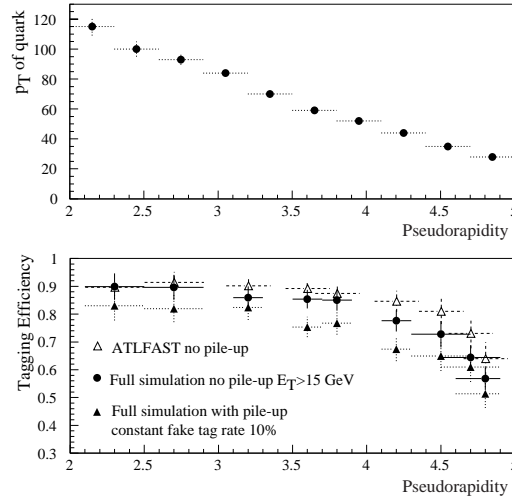**Fig. 12.** Feynman diagram for the Vector Boson Fusion process.

Fig. 13. Top Figure: Average p_T of the forward quarks produced in association with a 1 TeV Higgs. Bottom Figure: Jet tagging efficiency for particle level (ATLFAST) and full simulation at low luminosity for a 15 GeV E_T threshold and with high luminosity pile-up.

4 τ Jet Reconstruction

τ jets are jets originating from the hadronic decay of τ leptons. Since there are neutrinos and hadrons among the decay products it is difficult to efficiently reconstruct and identify τ jets. A number of benchmark processes depend upon

the ability to efficiently reconstruct and identify τ jets. These processes include the production of charged Higgs $H \to \tau\nu$, light Standard Model Higgs from Vector Boson Fusion $q\,q\,H \to q\,q\,\tau\,\tau$, and SUSY production $H/A \to \tau\,\tau$ at large $\tan\beta$. Figure 14 [3] demonstrates the accessible parameter space for the observation of $H/A \to \tau\,\tau$ within the Minimal Supersymmetric Standard Model at the LHC. Potential backgrounds include $Z \to \tau\,\tau$, $t\overline{t}$, $b\overline{b}$, and $W + jet(s)$ events.
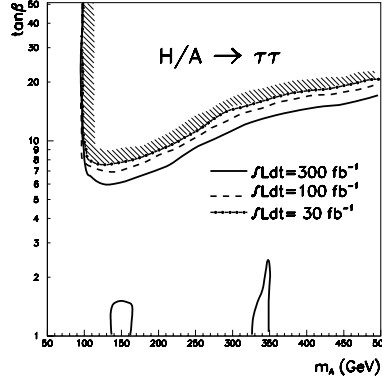

Fig. 14. The 5σ discovery contour curves for the $H/A \to \tau\tau$ channel in the $(m_A, \tan\beta)$ plane for several integrated luminosities.

τ jets can be identified through the presence of a well collimated calorimeter cluster and usually either 1 or 3 associated charged tracks. Three distinguishing variables help to efficiently identify τ jets from the backgrounds.

- R_{em}: the jet radius computed using only the electromagnetic calorimeter cells within $\Delta R = 0.7$ of the jet;

- ΔE_T^{12}: the fraction of E$_T$ in the electromagnetic and hadron calorimeters within an isolation region of $0.1 < \Delta R < 0.2$ around the jet;

- N_{tr}: the number of charged tracks pointing to the cluster within $\Delta R = 0.3$.

As can be seen from Figure 15 [3] the electromagnetic radius of τ jets (left) is significantly smaller than for QCD jets (right). Therefore, the fine granularity of the electromagnetic calorimeter is important for efficient τ jet tagging.

Figure 16 [3] demonstrates the expected jet rejection from simulation as a function of τ reconstruction efficiency in the search for $A \to \tau\tau$ events. A good level of τ/jet separation is expected over a broad p_T range. As expected for higher p_T τ's the τ identification efficiency increases for constant values of the jet rejection. For a τ identification efficiency of $\approx 20\%$ a rejection factor of 170-1200 can be achieved against jets from W+jets and $t\overline{t}$ events. An even larger rejection of ≈ 1700 is achieved against b jets. Overall, there is good sensitivity for the identification of τ's in many physics channels ranging from light Higgs to heavy SUSY.
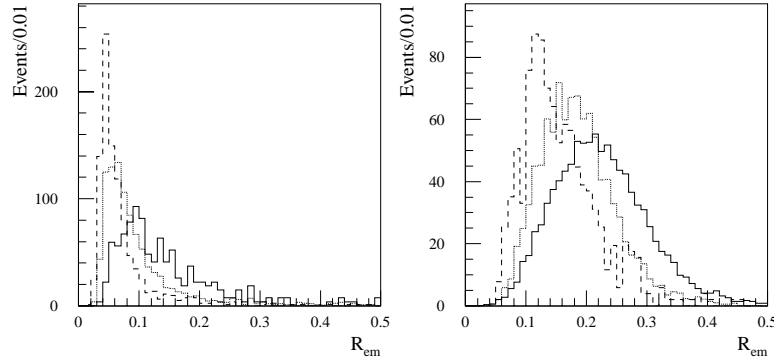
Fig. 15. Electromagnetic radius, R_{em}, for τ jets (left) and QCD jets (right) with different p_T ranges: $15 < p_T < 30$ GeV (full line), $30 < p_T < 70$ GeV (dotted line), $70 < p_T < 130$ GeV (dashed line).
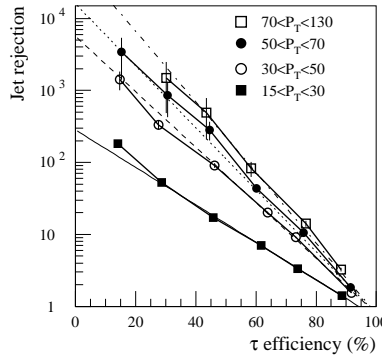

Fig. 16. Jet rejection as a function of the τ efficiency within $|\eta| < 2.5$ for various p_T ranges.

5   E$_T^{miss}$ Measurement

Missing transverse energy (E_T^{miss}) is an important signal for new physics, such as SUSY particle production and decay, at the LHC. Therefore, good measurement of E_T^{miss} within ATLAS is needed.

The aim is to minimize fake high-E_T^{miss} tails produced by instrumental effects such as poorly measured jets in a calorimeter crack. The detector must also have the ability to accurately reconstruct narrow invariant mass distributions for new particles with neutrinos among their decay products, such as from Vector Boson Fusion, $q\,q\,H \to q\,q\tau\,\tau \to l\,l\,\nu\,\nu$. In order to achieve these goals the ATLAS Calorimetry system must provide good energy resolution, good linearity of response, and hermetic coverage.

5.1   E$_T^{miss}$ Resolution

In order to provide good E_T^{miss} resolution the calorimeter calibration must account for energy loss in dead materials, such as the cryostats, and calorimeter transition regions where cracks may be present. When calculating the E_T^{miss} resolution cells containing low deposits of energy, above some threshold, are included. However, the calorimeter response to such low energy particles outside of clusters is relatively non-linear. Therefore, calibration, which includes the low energy cells outside of clusters, is important for the E_T^{miss} resolution.

The resolution at which the E_T^{miss} is measured also depends upon the level of electronic noise in the calorimeter. When taking electronic noise into account it was found that a cell energy cut-off of 1.5σ is optimal, and deteriorates the measured E_T^{miss} resolution by less than 10% (3 GeV) [3].

Good calorimeter coverage is also important. Figure 17 (left) [3] demonstrates the expected E_T^{miss} resolution as a function of the total observed E_T in the event for $A \to \tau\tau$ decays with $m_A = 150$ GeV. The E_T^{miss} resolution is 7 GeV, with contributions of 5 GeV, 4 GeV, and 3 GeV coming from the barrel, end-cap, and forward calorimeters, respectively. The contribution from each calorimeter region decreases with pseudorapidity because the average transverse energy decreases.

The resolution is also strongly affected by minimum bias events. The right plot of Figure 17 [3] demonstrates the expected degradation of E_T^{miss} resolution as a function of the number of minimum bias events added per bunch crossing. For the expected 24 minimum bias events per bunch crossing the E_T^{miss} resolution degrades by approximately 12 GeV. The validity of the physics models used in the simulations should be tested with data in ATLAS.
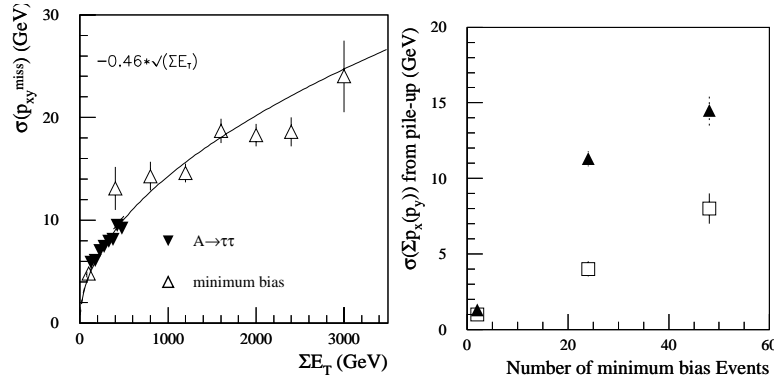

Fig. 17. Left Figure: Resolution of the two components of the E_T^{miss} vector, as a function of the total transverse energy in the calorimeters for minimum-bias events and $A \to \tau\tau$ events with $m_A = 150$ GeV at low luminosity. Right Figure: Contribution to $\sigma(p_{xy}^{miss})$ from the pile-up and electronic noise expected at high luminosity (closed symbols) and for the contribution of the FCAL alone (open symbols).

5.2   E$_T^{miss}$ Tails

The presence of missing energy is an important signature for new physics such as SUSY. It is therefore important to understand the effect of poorly reconstructed jets which may simulate large E_T^{miss} tails. To study this effect the production of Z+jet(s) events, where $Z \rightarrow \mu^+\mu^-$, is used. This process is a simple and well controlled channel, and well suited to the study of E_T^{miss} tails for all final states.

Figure 18 (left) [3] shows the E_T^{miss} distribution for events where the leading jet is undetected (solid line) and where the jets are fully simulated (dashed line). Only two events have genuine $E_T^{miss} > 200$ GeV due to the presence of high p_T neutrinos. Therefore a rejection factor of 1000 for events with fake missing transverse energy coming from poorly reconstructed jets is achieved. Figure 18 (right) [3] plots the pseudorapidity of the jet with the highest p_T for the events that have $E_T^{miss} > 50$ GeV. The jet energy resolution is degraded slightly in the region near $|\eta| \approx 1$ due to the vertical transition between the barrel and extended barrel calorimeters.
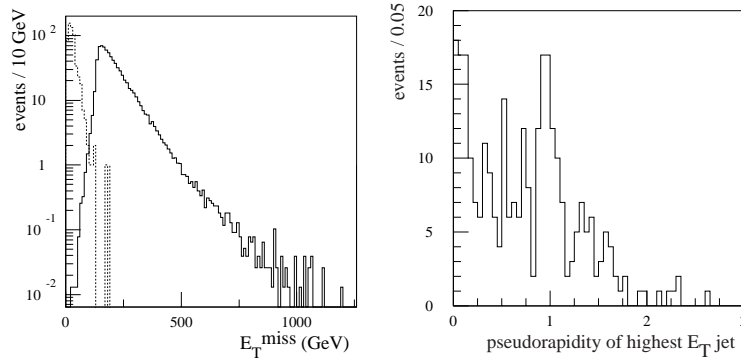

Fig. 18. Left Figure: E_T^{miss} distribution for Z+jet events with $p_T > 200$ GeV where the lead jet is undetected (full line) and for fully simulated events (dashed line). Right Figure: Pseudorapidity of the jet with the highest p_T for events with $E_T^{miss} > 50$ GeV.

6   Combined Performance

The ATLAS calorimetry has been shown to provide good measurements of jet energy resolution, τ identification and reconstruction, and E_T^{miss} resolution. Together these three areas are important to the overall combined performance of the ATLAS detector system for a variety of phyics processes.

Figure 19 [3] shows the reconstructed $W \rightarrow jj$ invariant mass from the search for a heavy Higgs boson ($m_H > 600$ GeV) in the decay channel $H \rightarrow WW \rightarrow l\nu jj$. Here the efficient reconstruction of high p_T W's is essential.

The reconstructed mass is 80.5 GeV and the resolution is 5.0 GeV (6.9 GeV) at low (high) luminosity. $W H$ production, followed by the decay $H \rightarrow b\bar{b}$, is a promising channel to observe a light Higgs boson at the LHC, both in the case of the Standard Model and of the MSSM. Figure 20 [3] shows the reconstructed invariant mass of the two b jets where both b's are reconstructed and have $p_T >$ 15 GeV. The mass resolution is $\sim$ 15 GeV. The reconstruction of $H/A \rightarrow \tau\tau$ decays requires good performance from the hadron calorimetry in terms of τ reconstruction as well as E_T^{miss} measurement. Figure 21 (left) [3] shows the reconstructed τ-pair mass spectrum from $H/A \rightarrow \tau\tau$ decays for $m_A = 150$ GeV.

At the LHC the top quark mass will be accurately measured using inclusive $t\bar{t}$ production. The production of $t\bar{t}$ pairs is also expected in several channels coming from new physics such as Higgs production and SUSY. In both cases good dijet and multi-jet mass resolution is needed, along with good calorimeter granularity to separate nearby jets. Figure 21 (right) [3] shows the reconstructed m_{jjb} distribution obtained by using the jjb combination which gives the highest p_T of the reconstructed top quark. The reconstructed m_{jjb} mass resolution is approximately 13 GeV.
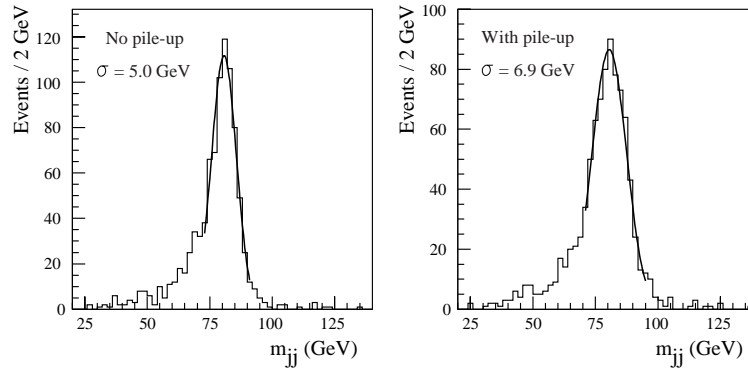

Fig. 19. Reconstructed W mass after applying a linear correction as a function of the p_T of the W at low luminosity (left) and with high luminosity pile-up included (right).

7   Conclusion

Jet, τ and E_T^{miss} physics is very important at the LHC. The physics goals of the LHC are very challenging and place stringent requirements upon the detector performance including the Calorimetry. The ATLAS Calorimetry system is able to satisfy these physics requirements with its strongest features of good energy resolution, hermeticity, and granularity.

Good jet energy calibration is possible from using the cell weighting method. In situ calibration for $W \rightarrow jj$ and Z+jet(s) events is also possible allowing for
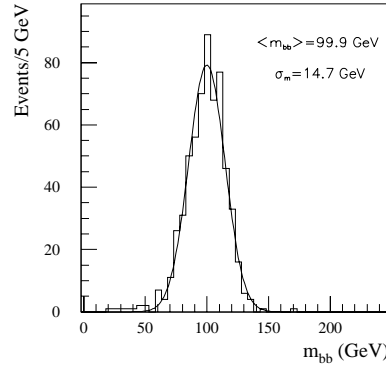
Fig. 20. Reconstructed invariant mass distribution of the two b-jets in the final state for $H \to b\bar{b}$ events with $M_H = 100$ GeV at low luminosity.

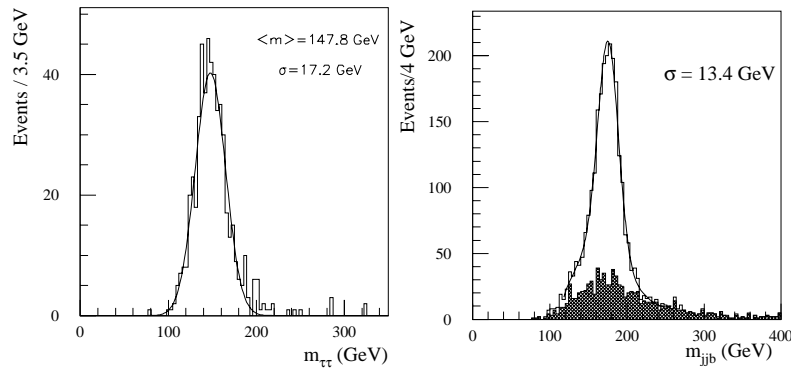**Fig. 21.** Left Figure: Reconstructed $A \to \tau\tau$ mass at low luminosity for $m_A = 150$ GeV. Right Figure: Invariant mass distribution of the accepted $j\,j\,b$ combinations from the fully-simulated inclusive $t\bar{t}$ sample. The shaded histogram shows the background from wrong combinations.

measurement of the absolute jet energy scale to an accuracy of 1%. The AT-LAS Calorimetry is also well suited for the task of forward jet tagging for Higgs production from Vector Boson Fusion. Hadronic τ decays can be efficiently reconstructed and identified from calorimeter and inner detector tracking information. The E_T^{miss} performance is very good and optimised through the application of a cell energy cut-off when including the effects of electronic noise and pile-up. No large E_T^{miss} tails are produced from high p_T jets in less uniform calorimeter regions.

Overall, ATLAS is well suited to take advantage of the large physics potential of the LHC.

References

1. "ATLAS Calorimeter Performance Technical Design Report", ATLAS Collaboration, CERN/LHCC/96-40, ATLAS TDR 1, 15 December 1996.
2. "ATLAS Tile Calorimeter TDR", ATLAS Collaboration, CERN/LHCC/96-42, 15 December 1996.
3. "Detector and Phyics Performance Technical Design Report" Volumes 1 and 2, ATLAS Collaboration, CERN/LHCC/99-14, ATLAS TDR 14, 25 May 1999.
4. H. Seymour, Z. Phys. **C62** 127 (1993).
5. R. Wigmans, Nucl. Instr. and Meth. **A259** (1988) 273.
6. B. Dowler *et al.*, Nucl. Instr. and Meth. **A482** (2002) 94.
7. D. Groom, VII International Conference on Calorimetry in High Energy Physics, Tuscon, Arizona, 9-14 November, 1997.